

Perturbation theory of quasinormal modes for geometrically deformed nanoresonators

Wei Yan,^{1,2,*} Philippe Lalanne,³ and Min Qiu^{1,2,†}

¹Key Laboratory of 3D Micro/Nano Fabrication and Characterization of Zhejiang Province, School of Engineering, Westlake University, 18 Shilongshan Road, Hangzhou 310024, Zhejiang Province, China

²Institute of Advanced Technology, Westlake Institute for Advanced Study, 18 Shilongshan Road, Hangzhou 310024, Zhejiang Province, China

³Laboratoire Photonique, Numérique et Nanosciences (LP2N), IOGS-Univ. Bordeaux-CNRS, 33400 Talence cedex, France

(Dated: September 11, 2022)

When material parameters are fixed, optical responses of nanoresonators are dictated by their geometric dimensions. Therefore, both designing nanoresonators and understanding their underlying physics would benefit from a theory that can predict the evolutions of resonance states of open systems—the so-called quasinormal modes (QNMs)—as the geometric dimensions of nanoresonators change. The QNM perturbation theories are the ideal choice. However, the existed theories are simply unable to deliver the correct perturbation series in terms of geometrical deformations, an issue due to field discontinuities across different media. In this letter, we solve this issue by proposing a new extrapolation technique to reconstruct electromagnetic fields in perturbed domains, then by linking geometrical deformations with surface polarizations. We exemplify the broad applications of the proposed theory by: (1) designing super-cavity modes and exceptional points with a superb efficiency as compared with the standard methodology that relies on brute-force simulations; (2) revealing extremely-localized gap-plasmon dynamics, particularly, highlighting the interplay between near-field contributions and quantum corrections.

In nanophotonics, nanoresonators are one of the fundamental devices to control light [1]. Besides material parameters, geometric dimensions provide another degree of freedom to manipulate the functionalities of nanoresonators. The exploitation of the geometric freedom in designing nanoresonators widely relies on brute-force simulations that scan a selected space of geometric parameters. Despite being robust, a purely-numerical approach is computationally expensive and lacks of physical insights; an alternative approach, with a better balance of physics and numerics, is desirable.

Due to their leaky character, resonance modes are termed as quasinormal modes (QNMs) having complex frequencies and diverging far fields [2–4]. With the correct normalization [2, 5, 6], a few dominantly-excited QNMs can well reconstruct nanoresonators' optical responses [4]. Theoretically, engineering the functionalities of nanoresonators is equivalent to deriving the explicit geometric dependence of QNMs, which here is formulated as a perturbation problem—*predicting QNMs of a complex nanoresonator from another geometrically different, simple one.*

The perturbation theory, a classical topic, has been recently generalized with the QNM concept [7–10]. Despite the existed theories apply well for tiny material changes, they fail to give the correct perturbation series when perturbation changes are large due to field discontinuities across different media [11]. Therefore, these theories cannot apply for the geometric deformation problem where the material changes—being proportional to the permittivity difference between nanoresonators and backgrounds—could be large. A recipe to solve this issue partly has been proposed in Ref. [11] using a smooth method, which, however, are sub-

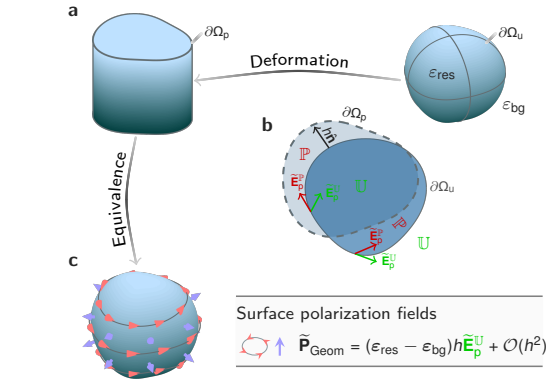


FIG. 1. **Scheme of the perturbation theory.** **a.** A nanoresonator with boundary $\partial\Omega_u$ is geometrically deformed to a new one with boundary $\partial\Omega_p$. **b.** The Geometric deformation is parameterized by $h\hat{\mathbf{n}}$, a shift from $\partial\Omega_u$ to $\partial\Omega_p$ along outward normal direction, $\hat{\mathbf{n}}$, of $\partial\Omega_u$. The perturbed domains between $\partial\Omega_u$ and $\partial\Omega_p$, where material parameters change after the deformation, are labelled by \mathbb{P} ; the unperturbed domains are labelled by \mathbb{U} . **c.** The perturbation theory bases on representing the perturbed resonator with the unperturbed one plus surface polarizations, $\tilde{\mathbf{P}}_{\text{Geom}}$, which locates at the boundary of $\partial\Omega_u$ on the *perturbed* side, while depending on the electric fields on the *unperturbed* side of $\partial\Omega_u$, denoted by $\tilde{\mathbf{E}}_p^u$.

ject to several constraints imposed by its departure from the normal mode concept and from non-dispersive and isotropic materials, and by its difficulty in extending for high-order perturbative analysis. We here completely remove all these constraints by developing a new QNM perturbation theory for the geometric deformation problem.

Theory—A (unperturbed) nanoresonator is geometrically deformed to a new (perturbed) one with the boundary $\partial\Omega_u$ changing to $\partial\Omega_p$ (Fig. 1a). The geometric deformation is parameterized by $h\hat{\mathbf{n}}$ measuring the shift from $\partial\Omega_u$ to $\partial\Omega_p$, where $\hat{\mathbf{n}}$ denotes unit outward normal vector of $\partial\Omega_u$ (Fig. 1b). The theory starts from the LippmanSchwinger integral equation that expresses the electric fields of the perturbed system, $\tilde{\mathbf{E}}_p$, with the Green's tensor of the unperturbed system, \mathbf{G}_u — $[\nabla \times \mu_0^{-1} \nabla \times -\omega^2 \boldsymbol{\varepsilon}_u] \mathbf{G}_u(\mathbf{r}, \mathbf{r}'; \omega) = \omega^2 \mathbf{I} \delta(\mathbf{r} - \mathbf{r}')$ — $\tilde{\mathbf{E}}_p(\mathbf{r}) = \iiint \mathbf{G}_u(\mathbf{r}, \mathbf{r}'; \omega) [\boldsymbol{\varepsilon}_p(\mathbf{r}'; \omega) - \boldsymbol{\varepsilon}_u(\mathbf{r}'; \omega)] \tilde{\mathbf{E}}_p(\mathbf{r}') d^3 \mathbf{r}'$ (see SI. Sec. I), where $\boldsymbol{\varepsilon}_{u,p}$ denote the permittivities of the unperturbed and perturbed systems, respectively. The conventional perturbation theories follow from expanding $\tilde{\mathbf{E}}_p$ with the electric fields of the QNMs of the unperturbed system, $\tilde{\mathbf{E}}_{u,n}$ (n , the eigenindex). Such an approach is unsuitable for the perturbation analysis. The fact can be appreciated by noticing that $\tilde{\mathbf{E}}_{u,n}$ is not a correct zeroth-order approximation to its perturbed counterpart, $\tilde{\mathbf{E}}_{p,n}$, since the normal component of $\tilde{\mathbf{E}}_{u,n}$ is discontinuous across $\partial\Omega_u$, while, for $\tilde{\mathbf{E}}_{p,n}$, the discontinuity occurs at $\partial\Omega_p$ instead.

(T1) Extrapolating Fields in the Perturbed Domain: To bypass the aforementioned issue, we abandon the conventional scheme and propose a new one. First, we disregard the perturbed domain between $\partial\Omega_u$ and $\partial\Omega_p$ (see the domain \mathbb{P} in Fig. 1b) for a moment, and perform the QNM expansion for $\tilde{\mathbf{E}}_p$ limited in the unperturbed domain where the QNM fields before and after the perturbation share the same continuity/discontinuity properties. After that, we take a key step that $\tilde{\mathbf{E}}_p$ in the perturbed domain is extrapolated by the Taylor series expansions employing $\tilde{\mathbf{E}}_p^u - \tilde{\mathbf{E}}_p$ at the *unperturbed* side of $\partial\Omega_u$, cf. Fig. 1b—and its derivatives: $\tilde{\mathbf{E}}_p(\mathbf{r}) = \sum_{j=0}^{\infty} (l^j/j!) \overleftarrow{\partial}_{\hat{\mathbf{n}}}^j \tilde{\mathbf{E}}_p^u(\mathbf{r}_{\Omega_u})$, where $\overleftarrow{\partial}_{\hat{\mathbf{n}}} \tilde{\mathbf{E}}_p^u(\mathbf{r}_{\Omega_u}) \equiv (\hat{\mathbf{n}} \cdot \nabla) \tilde{\mathbf{E}}_p^u(\mathbf{r}_{\Omega_u})$, and $\mathbf{r} \equiv l\hat{\mathbf{n}} + \mathbf{r}_{\Omega_u}$ with $l \in [0, h]$ and \mathbf{r}_{Ω_u} denoting coordinates of $\partial\Omega_u$. The extrapolation is justified because that the materials in the perturbed domain are as the same as at the unperturbed side of $\partial\Omega_u$, and the fields in a continuous domain with the same materials are analytic. With these considerations, the volume-integral LippmanSchwinger equation is transformed into a surface-integral one over $\partial\Omega_u$ (employing the Taylor series of $\tilde{\mathbf{E}}_p$ introduced above and of \mathbf{G}_u ; SI. Sec. II):

$$\tilde{\mathbf{E}}_p(\mathbf{r}) = \iint_{\partial\Omega_u} \mathbf{G}_u(\mathbf{r}, \mathbf{r}_{\Omega_u}; \omega) \tilde{\mathbf{P}}_{\text{Geom}}(\mathbf{r}_{\Omega_u}; \omega) da. \quad (1a)$$

The surface polarizations, $\tilde{\mathbf{P}}_{\text{Geom}}$ (Fig. 1c), locates at the perturbed side of $\partial\Omega_u$, and are expressed as

$$\tilde{\mathbf{P}}_{\text{Geom}} = \sum_{j=0}^{\infty} \sum_{k=0}^{\infty} \overleftarrow{\partial}_{\hat{\mathbf{n}}}^k \Delta \boldsymbol{\varepsilon} f_{jk} \overrightarrow{\partial}_{\hat{\mathbf{n}}}^j \tilde{\mathbf{E}}_p^u. \quad (1b)$$

Here, $\Delta \boldsymbol{\varepsilon} \equiv \boldsymbol{\varepsilon}_{\text{res}} - \boldsymbol{\varepsilon}_{\text{bg}}$, the difference between the permittivities of nanoresonators and background media; $f_{jk} =$

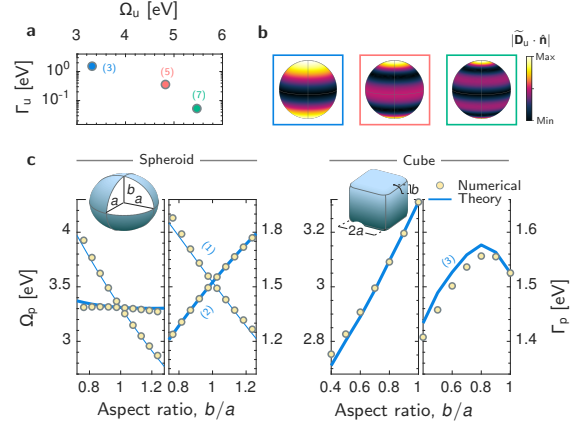


FIG. 2. Validation of the perturbation theory. A metallic sphere with a radius of 50 [nm] in air background is deformed to spheroids and cubes. The sphere has a Drude permittivity $\varepsilon_{\text{metal}} = 1 - \omega_p^2/(\omega^2 + i\omega\gamma)$ with $\hbar\omega_p = 9$ [eV] and $\gamma = 0.0023\omega_p$ close to Ag. **a.** Eigenfrequencies of dipole (blue), quadrupole (red), hexapole (green) plasmonic QNMs of the sphere, $\tilde{\omega}_u \equiv \Omega_u - i\Gamma_u/2$, including 15 QNMs with degeneracy factors labelled in parenthesis. **b.** Amplitudes of normal component of electric displacement fields at the metal-air boundary for dipole, quadrupole, hexapole (left to right) modes with azimuthal order $m = 0$. **c.** Eigenfrequencies of the metallic spheroids and cubes, $\tilde{\omega}_p \equiv \Omega_p - i\Gamma_p/2$, over a range of aspect ratios a/b with $a = 50$ [nm] (small deformations close to $a/b = 1$). The theoretical predictions (solid curves), with Eqs. (2) including 15 QNMs, exhibit an overall quantitative agreement with the numerical results obtained with the QNMEig [12] (circles).

$\frac{h^{k+j+1}}{k!j!} \left(\frac{1}{k+j+1} + \kappa_m \frac{2h}{k+j+2} + \kappa_g \frac{h^2}{k+j+3} \right)$, where $\kappa_{m,g}$ are the mean and Gaussian curvatures of $\partial\Omega_u$, respectively; $\overleftarrow{\partial}_{\hat{\mathbf{n}}}$ is defined such that $f(\mathbf{r}_{\Omega_u}) \overleftarrow{\partial}_{\hat{\mathbf{n}}} \equiv (\hat{\mathbf{n}} \cdot \nabla) f(\mathbf{r}_{\Omega_u})$.

Equations (1) are the cornerstone of the proposed perturbation theory. They define a new integral formulation for the perturbed fields, which allows us to derive a correct perturbation theory to arbitrary orders. They are completely different from the classical multi-pole expansion of the LippmanSchwinger equation, for which the equivalent of $\tilde{\mathbf{P}}_{\text{Geom}}$ depends on the electric fields at the *perturbed* side of $\partial\Omega_u$, and the resulted perturbation series are *inaccurate*.

(T2) Perturbation Theory: We perform the QNM expansions: $\tilde{\mathbf{E}}_p = \sum_n \alpha_n \tilde{\mathbf{E}}_{u,n}$, and $\mathbf{G}_u \Delta \boldsymbol{\varepsilon} = -\sum_m \tilde{\mathbf{E}}_{u,m} \otimes \tilde{\mathbf{E}}_{u,m} \left[\frac{\tilde{\omega}_{u,m} \Delta \boldsymbol{\varepsilon}(\tilde{\omega}_{u,m})}{\omega - \tilde{\omega}_{u,m}} + \Delta \boldsymbol{\varepsilon}_{\infty} \right]$ (see SI. Sec. III for derivations), where material dispersions are described by the Lorentz-Drude model, and $\Delta \boldsymbol{\varepsilon}_{\infty} \equiv \lim_{\omega \rightarrow \infty} \Delta \boldsymbol{\varepsilon}(\omega)$. Plugging these expansions into Eqs. (1), we arrive at a linear eigenvalue equation for the eigenstates of the perturbed system, $\{\tilde{\omega}_p, |\alpha\rangle\}$ ($|\alpha\rangle \equiv [\alpha_1; \alpha_2; \dots]$):

$$(\Omega_u - i\Gamma_u/2) \{ \mathbf{I} - [\mathcal{H}_\omega - \mathcal{H}_{\infty}] \} |\alpha\rangle = \tilde{\omega}_p [\mathbf{I} + \mathcal{H}_{\infty}] |\alpha\rangle. \quad (2a)$$

Here, \mathbf{I} denotes the identity matrix; Ω_u and Γ_u are the real-valued diagonal matrices with $\Omega_{u,mn} - i\Gamma_{u,mn}/2 = \tilde{\omega}_{u,m}$. For

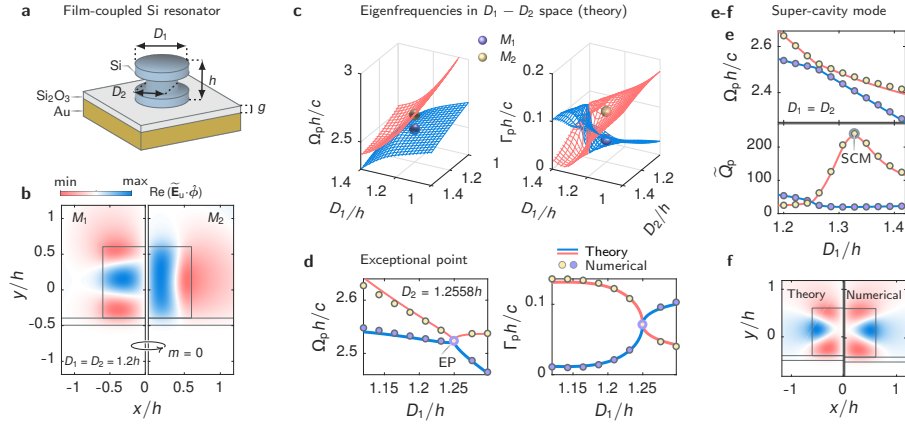


FIG. 3. **Application of the perturbation theory for designing exceptional points (EPs) and high- Q super-cavity modes (SCMs).** **a.** A silicon dumbbell-shaped nanoresonator with $\epsilon_{\text{Si}} = 13$ sits above an Au substrate gapped by a thin silica layer with refractive index of 1.45 and gap distance $g = 50$ [nm]. The silicon dumbbell consists of three equal-height cylinders (total height $h = 500$ [nm]), and diameters D_1 , D_2 and D_1 (from top to bottom). The Au permittivity is approximated by the Lorentz-Drude model $\epsilon_{\text{Au}}(\omega) = \epsilon_{\infty} - \omega_{p,1}^2/(\omega^2 + i\gamma_1\omega) - \omega_{p,2}^2/(\omega^2 - \omega_0^2 + i\gamma_2\omega)$ with $\epsilon_{\infty} = 6$, $\hbar\omega_{p,1} = 8.67$ [eV], $\hbar\gamma_1 = 0.1$ [eV], $\hbar\omega_{p,2} = 3.65$ [eV], $\hbar\gamma_2 = 2.15$ [eV], $\hbar\omega_0 = 7.38$ [eV]. **b.** Field distributions of azimuthal-component electric fields, $\text{Re}(\vec{E}_{u,\phi})$, of two modes M_1 and M_2 with azimuthal order $m = 0$ for the nanoresonator when $D_1 = D_2 = 1.2h$. **c.** Eigenfrequencies calculated with Eqs. (2) for perturbed QNMs resulting from the coupling of M_1 and M_2 as the parameter $D_1 - D_2$ is spanned. **d.** Eigenfrequencies of M_1 - M_2 coupled modes for $D_2 = 1.2558h$. The EP is labelled. **e.** Resonance frequencies and quality factors of M_1 - M_2 coupled modes for $D_1 = D_2$. The SCM with $\bar{Q}_p \approx 240$ is labelled in the lower panel. **f.** Field distributions of $\text{Re}(\vec{E}_{p,\phi})$ of the SCM. In **d-f**, the theory and numerical results show quantitative agreements.

convenience of numerical implementations and simplicity in analytical studies, while having an acceptable level of predictive force, we make the first-order approximation for the perturbation operator:

$$\mathcal{H}_{\omega,nq} \approx \langle \vec{E}_{u,n}^* | \hbar \Delta \epsilon(\bar{\omega}_{u,n}) | \vec{E}_{u,q}^u \rangle_{\partial\Omega_u}, \quad (2b)$$

where n and q are the matrix indices, and $\langle \mathbf{A}^* | \hat{\mathcal{O}} | \mathbf{B} \rangle_{\partial\Omega_u} \equiv \iint_{\partial\Omega_u} \mathbf{A}(\mathbf{r}_{\Omega_u}) \cdot \hat{\mathcal{O}}(\mathbf{r}_{\Omega_u}) \cdot \mathbf{B}(\mathbf{r}_{\Omega_u}) da$ is an overlap integral over $\partial\Omega_u$. \mathcal{H}_{ω} has a similar expression with $\Delta \epsilon(\bar{\omega}_{u,q})$ in Eq. (2b) replaced by $\Delta \epsilon_{\infty}$.

Equations (2) are the main result of this letter. Comparing with the existed theories [7–10], the essential difference here is that the perturbation operator \mathcal{H} depends not only on \vec{E}_u^p but also on \vec{E}_u^u . It is this difference rendering our theory the correct perturbation series, as later evidenced numerically. For a non-degenerated mode $\vec{E}_{u,n}$ the frequency shift $\Delta\bar{\omega}_n \equiv \bar{\omega}_{p,n} - \bar{\omega}_{u,n}$ up to the second-order terms of h^2 is expressed as

$$\Delta\bar{\omega}_n \approx -\mathcal{H}_{\omega,nn} + \mathcal{H}_{\omega,nn}^2 + \sum_q^{q \neq n} \frac{\bar{\omega}_{u,n}}{\bar{\omega}_{u,q} - \bar{\omega}_{u,n}} \mathcal{H}_{\omega,nq} \mathcal{H}_{\omega,qn}. \quad (3a)$$

Under several simplifications—assuming isotropic, non-dispersive materials, and in the limiting of the Hermitian physics, i.e., $\text{Im}(\bar{\omega}_{u,n}) \rightarrow 0$ and $\vec{E}_{u,n}$ being real valued—, the first term of Eq. (3a) reduces to the one in Ref. [11].

(T3) Validation: Consider a metallic Drude sphere in air background (see the caption of Fig. 2 for parameter details).

We deform the sphere to spheroids and cubes over a wide range of aspect ratios of a/b (Figs. 2c-d, insets); the two class of deformations reduce to sphere at $a/b = 1$. The QNMs of the cube and spheroid are predicted with Eq. (2) retaining the first 15 low-frequency plasmonic QNMs of the sphere, whose eigenfrequencies are shown in Fig. 2a with the degeneracy factors explicitly labelled, and whose representative mode profiles are plotted in Fig. 2b. Figure 2c present the eigenfrequencies of the QNMs of the perturbed geometries, $\bar{\omega}_p \equiv \Omega_p - i\Gamma_p/2$, as they depart from the initial dipole modes of the sphere (see the red circles in Fig. 2a for eigenfrequencies). The theoretical predictions (solid curves) show an overall quantitative agreement with the numerical results (circles) obtained directly by computing the QNM with the numerical solver QNMEig [12], particularly for small deformations close to $a/b = 1$. It should be known that this level of accuracy, with using a few QNMs, is unattainable with the previous theories [7, 9] (see SI. Sec. V).

Applications—The developed theory can find applications in various subareas of nanophotonics involving nanostructures that need to be engineered by tuning geometric dimensions. Below, we exemplify the application scope of our theory with two examples taken from two different topics: (A1) the first one concerns the design of special resonance modes, super-cavity modes [13] and exceptional points [14]; (A2) the other one aims at revealing the physics of extremely-localized gap plasmons [15–17].

(A1) Design: A general workflow for designing nanostructures

onators with the perturbation theory is as follows. Starting with a guessed nanoresonator, we compute its QNMs. Then, we vary the geometry of the starting nanoresonator—that is constrained by a set of user-defined geometric parameters, e.g., due to nanofabrication considerations—and compute the QNMs of the new resonators with Eqs. (2). The numerical efficiency is gained at this step since the computation of Eqs. (2)—which usually include a few QNMs—is almost instantaneous. An optimized nanoresonator, whose optical responses inferred from the computed QNMs match best our targets, is identified. We can further iterate the above steps until the optimized geometric parameters converge.

We illustrate our purpose by designing super-cavity modes (SCMs) and exceptional points (EPs). SCMs are the analogue of bound states in the continuum (BIC) for finite-size structures, having high Q values due to destructive interferences of radiations [13], while EPs with two or more states coalescing may lead to novel applications in lasing [18] and sensing [19]. Physically, both SCMs and EPs can be constructed in a two-mode coupled system by carefully tuning modal coupling constants, e.g., by varying geometric dimensions. We here consider a Si dumbbell-shaped nanoresonator deposited on an Au substrate coated with a Si_2O_3 film (thickness $g = 50$ [nm]). The diameter parameters of the Si dumbbell, D_1 and D_2 (see Fig. 3a), are freely adjusted for searching SCMs and EPs. Our design begins with a guessed nanoresonator with $D_1 = D_2 = 1.2h$ ($h = 500$ [nm]), for which we compute the QNMs. We then select two QNMs, denoted by M_1 and M_2 —that are sufficiently frequency-protected with others, i.e., $|\bar{\omega}_{u;n} - \bar{\omega}_{u;M_i}| \gg |\mathcal{H}_{nM_i}|$, where $n \notin \{M_1, M_2\}$ —, defining a nearly perfect two-mode coupled system. Figure 3b shows the modal profiles of $M_{1,2}$, and both have the azimuthal order $m = 0$. By varying D_1 and D_2 , we compute the eigenfrequencies of the M_1 - M_2 coupled system with Eqs. (2), as shown in Fig. 3c. An EP is identified close to $D_1 = 1.250h$ and $D_2 = 1.256h$, see Fig. 3d for the coalescence of the two eigenvalues. On the other hand side, SCMs, revealed by their high- Q values, can be achieved with more relaxed geometric conditions than EPs. For instance, constraining $D_1 = D_2$, we observe in Fig. 3e that \bar{Q}_p of one mode significantly increases as D_1 increases and reach the maximum, $\bar{Q}_p \approx 240$ —that is higher than a Si rod in air by a factor of 1/5 [13]—, thereby identifying a SCM (see Fig. 3f for its modal profiles).

(A2) Extreme Plasmonics: The physics of nanoresonators often depends on very few critical geometric parameters. A popular methodology to reveal this dependence relies on frequency-domain simulations of optical responses, which, however, accesses the physics indirectly. The developed perturbation theory establishes an alternative methodology qualifying the same mission, while own a unique advantage of interpreting the physics straightforwardly. We here elucidate this application by considering a challenge example—gapped plasmonic systems, in which the emerg-

ing physics—extreme field localizations and quantum effects of electrons [15–17]—depends on a single parameter, gap thickness. Concretely, we consider two structures, (a) Au sphere dimers and (b) film-coupled Au nanodisks on Au substrates (Fig. 4a-b), and we study the extremely confined gap plasmons in both the classical and quantum regimes.

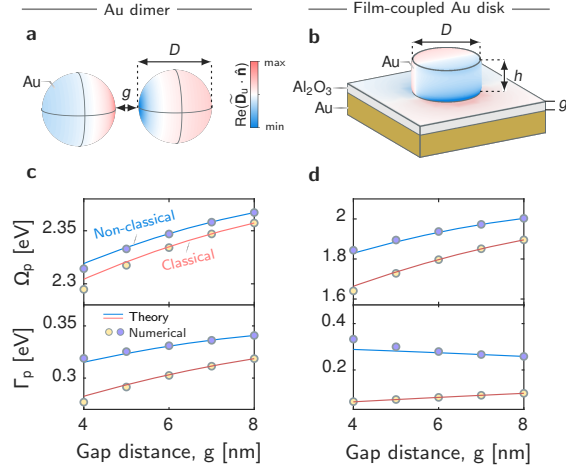


FIG. 4. Application of the perturbation theory for extremely-localized gap plasmons. **a-b.** Mode profiles $\text{Re}(\bar{\mathbf{D}}_u \cdot \hat{\mathbf{n}})$ for dipole gap-plasmon modes of two representative gap plasmonic structures: (a) Au sphere dimer with diameter $D = 60$ [nm]; (b) an Au disk with diameter $D = 60$ [nm] on an Au substrate covered by a thin dielectric ($\epsilon_{\text{Al}_2\text{O}_3} = 1.5$ [16]) film with gap distance $g = 8$ [nm]. The Au permittivity is detailed in the caption of Fig. 3. **c-d.** Eigenfrequencies $\bar{\omega}_p \equiv \Omega_p - i\Gamma_p/2$ of gap plasmons as the gap thickness is varied. For both the classical and quantum (non-classical) scenarios, the perturbation theory gives accurate results (solid curves) with Eqs. (3a) [classical] and (3b) [quantum], agreeing well with the numerical data (circles); the unperturbed resonator has gap distance $g = 8$ [nm]. Importantly, the off-diagonal near-field coupling between the gap plasmon of our interest and the other plasmons are retained in Eqs. (3) for a good numerical accuracy.

In the classical regime, the perturbation theory tells us that, as nanoresonators change their geometric dimensions, QNMs change due to the couplings with (1) themselves and (2) the other modes, cf. Eq. (3a). The second coupling—which we name as *the off-diagonal coupling* since it, mathematically, corresponds to the off-diagonal components of the perturbation operator \mathcal{H} —is generally negligible. However, for the gapped plasmonic systems, the off-diagonal coupling term is significant, manifesting itself in that the resonance frequency of the fundamental gap-plasmon modes (see Fig. 4a-b for modal profiles) exhibits a nonlinear dependence over the gap distance of a few nanometers, as observed in the top panels of Fig. 4c-d. We numerically find that the off-diagonal coupling is dominantly contributed from the plasmon modes that are well confined in the gap and, thus, strongly interact with each other via their near fields as the gap varies. This

finding is exploited to safeguard the prediction force of the perturbation theory, i.e., including the off-diagonal coupling of the plasmon modes in Eq. (3a). Figure 4c-d demonstrate good agreements between the numerical results of the classical eigenfrequencies (yellow circles) and the theoretical predictions with Eq. (3a) (red curves), for which we choose the unperturbed resonator with gap distance $g = 8$ [nm].

On top of the classical theory, we now include the quantum effects of electrons—chiefly, the nonlocality and the electron spill-out that become noticeable as the gap distance reduces below ~ 10 [nm]—using the Feibelman d_{\perp} parameter [20, 21], the centroid of the induced microscopic charge. The quantum effects have a simple geometric interpretation, i.e., shifting the metal-dielectric boundary by $\text{Re}(d_{\perp})\hat{\mathbf{n}}$, which is equivalently a geometrical deformation, and, thus, amounts to introduce a quantum-originated surface polarization $P_Q = (\epsilon_{\text{res}} - \epsilon_{\text{bg}})(\hat{\mathbf{E}}_p^{\text{U}} \cdot \hat{\mathbf{n}})d_{\perp}\hat{\mathbf{n}}$ at the metal-dielectric boundary [22]. Summing P_Q and P_{Geom} , the perturbation theory can be straightforwardly generalized to characterize both geometric deformations and quantum effects simultaneously. The overall frequency shift $\Delta\tilde{\omega}_m^Q$ is given as

$$\Delta\tilde{\omega}_n^Q \simeq \Delta\tilde{\omega}_n - Q_{\tilde{\omega}_n} + 2\mathcal{H}_{\tilde{\omega}_n}Q_{\tilde{\omega}_n} + \sum_{q \neq n} \frac{\tilde{\omega}_{u;n}}{\tilde{\omega}_{u;n} - \tilde{\omega}_{u;q}} (\mathcal{H}_{\tilde{\omega}_n}Q_{\tilde{\omega}_q} + Q_{\tilde{\omega}_n}\mathcal{H}_{\tilde{\omega}_q}). \quad (3b)$$

Here the first term $\Delta\tilde{\omega}_m$ given in Eq. (3a) represents the frequency shift due to the geometric changes, while the remaining terms account for the quantum corrections; the quantum-perturbation operator Q has the same expression as \mathcal{H} except that $h\Delta\epsilon$ is replaced by $d_{\perp}\hat{\mathbf{n}}(\hat{\mathbf{n}} \cdot \Delta\epsilon \cdot \hat{\mathbf{n}})\hat{\mathbf{n}}$ and the overlap integral is performed over the metal-dielectric boundary, cf. Eq. (2b).

Back to the gapped plasmonic systems, many experiments have observed that the quantum corrections increase as the gap distance decreases. This phenomenon can be simply interpreted with the second line of Eq. (3b), i.e., due to the coupling between the gap plasmon mode and the other plasmon modes mediated by both the geometric perturbation \mathcal{H} and the quantum perturbation Q . This interpretation is confirmed numerically in Fig. 4 c-d, where we see good agreements between the numerical results of the quantum-corrected eigenfrequencies (purple circles; $d_{\perp} = -0.5 + i0.3$ [nm] [16]) and the theoretical predictions with Eq. (3b) (blue curves), including the off-diagonal coupling between the gap plasmon of our interest and the other plasmon modes.

Conclusions—The proposed perturbation theory establishes a general framework for predicting the changes of QNMs as the geometric dimensions of nanoresonators change. Comparing with the fully-numerical approaches, our theory has the advantages of both numerical efficiency and physical transparency, thereby being a useful tool, particularly, for designing nanoresonators and revealing their physics, as evidenced with the numerical examples.

Acknowledgements—This project was supported by the National Key Research and Development Program of China (2017YFA0205700), the National Natural Science Foundation of China (61425023).

* wyanzju@gmail.com

† qiumin@westlake.edu.cn

- [1] L. Novotny, *Principles of Nano-Optics* (Cambridge University Press, Cambridge, 2012).
- [2] P. Leung, S. Liu, and K. Young, *Phys. Rev. A* **49**, 3057 (1994).
- [3] P. T. Kristensen, C. v. Vlack, and S. Hughes, *Opt. Lett.* **37**, 1649 (2012).
- [4] P. Lalanne, W. Yan, V. Kevin, C. Sauvan, and J.-P. Hugonin, *Laser Photonics Rev.* **4**, 1700113 (2018).
- [5] C. Sauvan, J.-P. Hugonin, I. S. Maksymov, and P. Lalanne, *Phys. Rev. Lett.* **110**, 237401 (2013).
- [6] E. A. Muljarov and W. Langbein, *Phys. Rev. B* **94**, 235438 (2016).
- [7] E. A. Muljarov, W. Langbein, and R. Zimmermann, *Europhys. Lett.* **92**, 50010 (2010).
- [8] J. Yang, H. Giessen, and P. Lalanne, *Nano Lett.* **15**, 3439 (2015).
- [9] T. Weiss, M. Mesch, M. Schäferling, H. Giessen, W. Langbein, and E. A. Muljarov, *Phys. Rev. Lett.* **116**, 237401 (2016).
- [10] K. G. Cognée, W. Yan, F. L. China, D. Balestri, F. Intonti, M. Gurioli, A. F. Koenderink, and P. Lalanne, *Optica* **6**, 269 (2019).
- [11] S. G. Johnson, M. Ibanescu, M. A. Skorobogatiy, O. Weisberg, and J. Joannopoulos, *Phys. Rev. B* **65**, 066611 (2002).
- [12] W. Yan, R. Faggiani, and P. Lalanne, *Phys. Rev. B* **97**, 205422 (2018).
- [13] M. Rybin, K. Koshelev, Z. Sadrieva, K. Samusev, A. Bogdanov, M. Limonov, and Y. Kivshar, *Phys. Rev. Lett.* **119**, 243901 (2017).
- [14] T. Kato, *Perturbation theory for linear operators* (Springer Science & Business Media, Berlin, 1972).
- [15] C. Ciraci, R. T. Hill, J. J. Mock, Y. Urzhumov, A. I. Fernández-Domínguez, S. A. Maier, J. B. Pendry, A. Chilkoti, and D. R. Smith, *Science* **337**, 1072 (2012).
- [16] Y. Yang, D. Zhu, W. Yan, A. Agarwal, M. Zheng, J. D. Joannopoulos, P. Lalanne, P. Lalanne, T. Christensen, K. K. Berggren, and M. Soljačić, arXiv:1901.03988 (2019).
- [17] K. J. Savage, M. M. Hawkeye, R. Esteban, A. G. Borisov, J. Aizpurua, and J. J. Baumberg, *Nature* **491**, 574 (2012).
- [18] F. Wong, Z. Ma, R. Wang, and X. Zhang, *Science* **346**, 972975 (2014).
- [19] W. Chen, S. Özdemir, G. Zhao, J. Wiersig, and L. Yang, *Nature* **448**, 192196 (2017).
- [20] P. J. Feibelman, *Prog. Surf. Sci.* **12**, 287 (1982).
- [21] W. Yan, M. Wubs, and N. Mortensen, *Phys. Rev. Lett.* **15**, 137403 (2015).
- [22] T. Christensen, W. Yan, A.-P. Jauho, M. Soljačić, and N. Mortensen, *Phys. Rev. Lett.* **118**, 157402 (2017).

SUPPLEMENTARY MATERIAL

Wei Yan,^{1,2,*} Philippe Lalanne,³ and Min Qiu^{1,2,†}

¹Key Laboratory of 3D Micro/Nano Fabrication and Characterization of Zhejiang Province, School of Engineering, Westlake University, 18 Shilongshan Road, Hangzhou 310024, Zhejiang Province, China

²Institute of Advanced Technology, Westlake Institute for Advanced Study, 18 Shilongshan Road, Hangzhou 310024, Zhejiang Province, China

³Laboratoire Photonique, Numérique et Nanosciences (LP2N), IOGS-Univ. Bordeaux-CNRS, 33400 Talence cedex, France

CONTENTS

I. LippmanSchwinger Formalism	1	IV. Comments on Conventional Perturbation Theories	4
II. Derivations of Eqs. (1)	1	References	5
III. Derivations of QNM Expansions of $G_u(\epsilon_{\text{res}} - \epsilon_{\text{bg}})$	2		

I. LIPPMANSCHWINGER FORMALISM

The LippmanSchwinger formalism expresses the electric fields of one system using the Green's tensor of another one. In this section, we present the derivations for the LippmanSchwinger formalism.

In the perturbed system (as defined in the main text), the source-free electric fields satisfy

$$\left[\nabla \times \mu_0^{-1} \nabla \times - \omega^2 \epsilon_p(\mathbf{r}; \omega) \right] \tilde{\mathbf{E}}_p(\mathbf{r}; \omega) = 0. \quad (\text{S.1.1a})$$

We reorganize Eq. (S.1.1a) into Eq. (S.1.1b) that manifests the evolution from the unperturbed system to the perturbed one.

$$\left[\nabla \times \mu_0^{-1} \nabla \times - \omega^2 \epsilon_u(\mathbf{r}; \omega) \right] \tilde{\mathbf{E}}_p(\mathbf{r}; \omega) = \omega^2 \left[\epsilon_p(\mathbf{r}; \omega) - \epsilon_u(\mathbf{r}; \omega) \right] \tilde{\mathbf{E}}_p(\mathbf{r}; \omega). \quad (\text{S.1.1b})$$

Then, we define the Green's tensor of the unperturbed system, G_u , with

$$\left[\nabla \times \mu_0^{-1} \nabla \times - \omega^2 \epsilon_u(\mathbf{r}; \omega) \right] G_u(\mathbf{r}, \mathbf{r}'; \omega) = \omega^2 I \delta(\mathbf{r} - \mathbf{r}'), \quad (\text{S.1.2})$$

where I denotes the second-rank identity tensor. Combining Eq. (S.1.2) and (S.1.1b) gives us

$$\tilde{\mathbf{E}}_p(\mathbf{r}; \omega) = \iiint G_u(\mathbf{r}, \mathbf{r}'; \omega) \left[\epsilon_p(\mathbf{r}'; \omega) - \epsilon_u(\mathbf{r}'; \omega) \right] \tilde{\mathbf{E}}_p(\mathbf{r}'; \omega) d^3 \mathbf{r}', \quad (\text{S.1.3})$$

which is the LippmanSchwinger formalism, departing from which we derive the perturbation theory in the main text.

II. DERIVATIONS OF EQS. (1)

In this section, we present the derivation details for Eqs. (1) in the main text. First, we recall that $\tilde{\mathbf{E}}_p$, in the perturbed domain where $\epsilon_p \neq \epsilon_u$, is constructed by the Taylor series expansion using $\tilde{\mathbf{E}}_p^U - \tilde{\mathbf{E}}_p$ at the unperturbed side of $\partial\Omega_u$, cf. Fig. 1b in the main text—and its derivatives:

$$\tilde{\mathbf{E}}_p(\mathbf{r}; \omega) = \sum_{j=0}^{\infty} \frac{l^j}{j!} \vec{\partial}_{\hat{\mathbf{n}}}^j \tilde{\mathbf{E}}_p^U(\mathbf{r}_{\Omega_u}; \omega), \quad (\text{S.2.1})$$

where $\mathbf{r} = l\hat{\mathbf{n}} + \mathbf{r}_{\Omega_u}$ with $l \in [0, h]$, \mathbf{r}_{Ω_u} denoting the coordinates of $\partial\Omega_u$ and $\hat{\mathbf{n}}$ denoting the unit outward normal vector of $\partial\Omega_u$; $\vec{\partial}_{\hat{\mathbf{n}}} \tilde{\mathbf{E}}_p^U(\mathbf{r}_{\Omega_u}) \equiv (\hat{\mathbf{n}} \cdot \nabla) \tilde{\mathbf{E}}_p^U(\mathbf{r}_{\Omega_u})$. Eq. (S.1.3), together with Eq. (S.2.1), results in Eqs.

(1) in the main text with the following algebra manipulations.

$$\begin{aligned}
\widetilde{\mathbf{E}}_p(\mathbf{r}; \omega) &\stackrel{a}{=} \sum_{j=0}^{\infty} \iiint \mathbf{G}_u(\mathbf{r}, \mathbf{r}'; \omega) [\boldsymbol{\varepsilon}_p(\mathbf{r}'; \omega) - \boldsymbol{\varepsilon}_u(\mathbf{r}'; \omega)] \frac{l'^j \rightarrow^j}{j!} \overleftarrow{\partial}_{\hat{\mathbf{n}}} \widetilde{\mathbf{E}}_p^U(\mathbf{r}'_{\Omega_u}; \omega) d^3 \mathbf{r}' \\
&\stackrel{b}{=} \sum_{k=0}^{\infty} \sum_{j=0}^{\infty} \iiint \mathbf{G}_u(\mathbf{r}, \mathbf{r}'_{\Omega_u}; \omega) \overleftarrow{\partial}_{\hat{\mathbf{n}}}^k [\boldsymbol{\varepsilon}_p(\mathbf{r}'; \omega) - \boldsymbol{\varepsilon}_u(\mathbf{r}'; \omega)] \frac{l'^{k+j} \rightarrow^j}{k! j!} \overleftarrow{\partial}_{\hat{\mathbf{n}}} \widetilde{\mathbf{E}}_p^U(\mathbf{r}'_{\Omega_u}; \omega) d^3 \mathbf{r}' \\
&\stackrel{c}{=} \sum_{k=0}^{\infty} \sum_{j=0}^{\infty} \iint_{\partial \Omega_u} \int_0^{h(\mathbf{r}'_{\Omega_u})} \mathbf{G}_u(\mathbf{r}, \mathbf{r}'_{\Omega_u}; \omega) \overleftarrow{\partial}_{\hat{\mathbf{n}}}^k [\boldsymbol{\varepsilon}_{\text{res}}(\omega) - \boldsymbol{\varepsilon}_{\text{bg}}(\omega)] \frac{l'^{k+j} \rightarrow^j}{k! j!} \overleftarrow{\partial}_{\hat{\mathbf{n}}} \widetilde{\mathbf{E}}_p^U(\mathbf{r}'_{\Omega_u}; \omega) [1 + l' \kappa_1(\mathbf{r}'_{\Omega_u})] [1 + l' \kappa_2(\mathbf{r}'_{\Omega_u})] dadl' \\
&\stackrel{d}{=} \sum_{k=0}^{\infty} \sum_{j=0}^{\infty} \iint_{\partial \Omega_u} \mathbf{G}_u(\mathbf{r}, \mathbf{r}'_{\Omega_u}; \omega) \overleftarrow{\partial}_{\hat{\mathbf{n}}}^k [\boldsymbol{\varepsilon}_{\text{res}}(\omega) - \boldsymbol{\varepsilon}_{\text{bg}}(\omega)] \frac{h(\mathbf{r}'_{\Omega_u})^{j+k+1}}{k! j!} \\
&\quad \left[\frac{1}{k+j+1} + \kappa_m(\mathbf{r}'_{\Omega_u}) \frac{2h(\mathbf{r}'_{\Omega_u})}{k+j+2} + \kappa_g(\mathbf{r}'_{\Omega_u}) \frac{h^2(\mathbf{r}'_{\Omega_u})}{k+j+3} \right] \overleftarrow{\partial}_{\hat{\mathbf{n}}} \widetilde{\mathbf{E}}_p^U(\mathbf{r}'_{\Omega_u}) da \\
&\stackrel{e}{=} \iint_{\partial \Omega_u} \mathbf{G}_u(\mathbf{r}, \mathbf{r}'_{\Omega_u}; \omega) \widetilde{\mathbf{P}}_{\text{Geom}}(\mathbf{r}'_{\Omega_u}; \omega) da
\end{aligned} \tag{S.2.2}$$

The above derivation involves the following steps:

- a. Inserting Eq. (S.2.1) into Eq. (S.1.3) and using the identity $\mathbf{r}' = l' \hat{\mathbf{n}} + \mathbf{r}'_{\Omega_u}$ defined above.
- b. Employing the Taylor series expansion for $\mathbf{G}_u(\mathbf{r}, \mathbf{r}'; \omega)$:

$$\begin{aligned}
\mathbf{G}_u(\mathbf{r}, \mathbf{r}'; \omega) &= \sum_{k=0}^{\infty} \left[\frac{\partial \mathbf{G}_u(\mathbf{r}, \mathbf{r}'_{\Omega_u}; \omega)}{\partial x'} n_x(\mathbf{r}'_{\Omega_u}) + \frac{\partial \mathbf{G}_u(\mathbf{r}, \mathbf{r}'_{\Omega_u}; \omega)}{\partial y'} n_y(\mathbf{r}'_{\Omega_u}) + \frac{\partial \mathbf{G}_u(\mathbf{r}, \mathbf{r}'_{\Omega_u}; \omega)}{\partial z'} n_z(\mathbf{r}'_{\Omega_u}) \right]^k \frac{l'^k}{k!} \\
&\equiv \sum_{k=0}^{\infty} \mathbf{G}_u(\mathbf{r}, \mathbf{r}'_{\Omega_u}; \omega) \overleftarrow{\partial}_{\hat{\mathbf{n}}}^k \frac{l'^k}{k!},
\end{aligned}$$

where $n_{x,y,z}$ denote the three Cartesian components of $\hat{\mathbf{n}}$, and $\mathbf{G}_u(\mathbf{r}, \mathbf{r}'_{\Omega_u}; \omega) \overleftarrow{\partial}_{\hat{\mathbf{n}}}^k$ is the shorthand notation for the derivative terms associated with \mathbf{G}_u . Noting that the Taylor series expansion of $\mathbf{G}_u(\mathbf{r}, \mathbf{r}'; \omega)$ is meaningful because we here restrict \mathbf{r} in the unperturbed domain with $|\mathbf{r} - \mathbf{r}'| \neq 0$, thereby ensuring that \mathbf{G}_u is analytic with respect to \mathbf{r}' .

- c. (1) Application of the identity $d^3 \mathbf{r}' = [1 + l' \kappa_1(\mathbf{r}'_{\Omega_u})] [1 + l' \kappa_2(\mathbf{r}'_{\Omega_u})] dadl'$, where $\kappa_{1,2}$ denotes the two principal curvatures of Ω_u , and da denotes the infinitesimal area element of Ω_u . (2) Application of the identity $\boldsymbol{\varepsilon}_p - \boldsymbol{\varepsilon}_u = [\boldsymbol{\varepsilon}_{\text{res}} - \boldsymbol{\varepsilon}_{\text{bg}}] \text{sgn}(h)$, where sgn denotes the sign function that is taken into account by setting the integral direction of dl' to be $\int_0^h \dots dl'$.
- d. Integrating out the variable l' , and using the definitions for the mean curvature κ_m and Gaussian curvature κ_g , i.e., $\kappa_m \equiv \kappa_1/2 + \kappa_2/2$ and $\kappa_g \equiv \kappa_1 \kappa_2$.
- e. Application of the definition of $\widetilde{\mathbf{P}}_{\text{Geom}}$, i.e., Eq. (1b) in the main text.

III. DERIVATIONS OF QNM EXPANSIONS OF $\mathbf{G}_u(\boldsymbol{\varepsilon}_{\text{res}} - \boldsymbol{\varepsilon}_{\text{bg}})$

The QNM expansions of $\mathbf{G}_u(\boldsymbol{\varepsilon}_{\text{res}} - \boldsymbol{\varepsilon}_{\text{bg}})$ are used to derive Eqs. (2) in the main text. In the literatures, one can find several simple expressions of the QNM expansions of \mathbf{G}_u , e.g., $\mathbf{G}_u = -\sum_n \widetilde{\mathbf{E}}_{u,n} \otimes \widetilde{\mathbf{E}}_{u,n} / (\omega - \widetilde{\omega}_{u,n})$. However, when materials are dispersive, the direct using of these expressions could result in that $\mathbf{G}_u[\boldsymbol{\varepsilon}_{\text{res}} - \boldsymbol{\varepsilon}_{\text{bg}}]$ exhibits a complex ω -dependence. Consequently, the eigenvalue equation for the perturbed problem is nonlinear, which is difficult. To overcome this difficulty, we here derive an alternative QNM-expansion expression for $\mathbf{G}_u[\boldsymbol{\varepsilon}_{\text{res}} - \boldsymbol{\varepsilon}_{\text{bg}}]$, being free of the complex ω -dependence imparted by material dispersions.

Firstly, we assume that ϵ_{res} and ϵ_{bg} are both described by the N -pole Lorentz-Drude model

$$\epsilon(\omega) = \epsilon_{\infty} \left(1 - \sum_{i=1}^N \frac{\omega_{p,i}^2}{\omega^2 - \omega_{0,i}^2 + i\omega\gamma_i} \right). \quad (\text{S.3.1})$$

ϵ_{res} and ϵ_{bg} have the same $\omega_{0,i}$ and γ_i , but different ϵ_{∞} and $\omega_{p,i}$. Note that if $\epsilon_{\text{res}}/\epsilon_{\text{bg}}$ is dispersionless, the associated $\omega_{p,i}$'s are zero. With Eq. (S.3.1), $\epsilon_{\text{res}} - \epsilon_{\text{bg}}$ are denoted by

$$\epsilon_{\text{res}}(\omega) - \epsilon_{\text{bg}}(\omega) \equiv \Delta\epsilon_{\infty} - \sum_{i=1}^N \frac{\Delta(\epsilon_{\infty}\omega_{p,i}^2)}{\omega^2 - \omega_{0,i}^2 + i\omega\gamma_i}. \quad (\text{S.3.2})$$

For the i -th Lorentz-pole, we introduce two auxiliary fields \mathbf{P}_i and \mathbf{J}_i defined by

$$\mathbf{P}_i \equiv -\epsilon_{\infty} \frac{\omega_{p,i}^2}{\omega^2 - \omega_{0,i}^2 + i\omega\gamma_i} \mathbf{E}, \quad \mathbf{J}_i \equiv -i\omega\mathbf{P}_i. \quad (\text{S.3.3})$$

Secondly, we associate $\mathbf{G}_u(\epsilon_{\text{res}} - \epsilon_{\text{bg}})$ with a concrete problem—computing the electric fields radiated by an electric current source $-i\omega[\epsilon_{\text{res}}(\omega) - \epsilon_{\text{bg}}(\omega)]\mathbf{S}_{\text{ext}}(\mathbf{r})$ in the unperturbed system, where \mathbf{S}_{ext} is an arbitrary function depending on space. Specifically, the total electric fields \mathbf{E} is given as

$$\mathbf{E} = \iiint \mathbf{G}_u(\mathbf{r}, \mathbf{r}'; \omega) [\epsilon_{\text{res}}(\omega) - \epsilon_{\text{bg}}(\omega)] \mathbf{S}_{\text{ext}}(\mathbf{r}') d^3\mathbf{r}'. \quad (\text{S.3.4})$$

Therefore, we see that the original problem of deriving the QNM expansions of $\mathbf{G}_u[\epsilon_{\text{res}} - \epsilon_{\text{bg}}]$ transforms to derive the QNM expansions of \mathbf{E} .

We define the augmented electromagnetic vector $\Psi = [\mathbf{H}, \mathbf{E}, \mathbf{P}, \mathbf{J}]$. Moreover, in order to simplify notations in the following derivations, we assume that dispersive permittivities only have one Lorentz pole; the extensions to the N -pole case are straightforward. Combining the Maxwell's equations and the definitions of the auxiliary fields gives

$$\begin{pmatrix} 0 & -i\mu_0^{-1}\nabla\times & 0 & 0 \\ i\epsilon_{\infty}^{-1}\nabla\times & 0 & 0 & -i\epsilon_{\infty}^{-1} \\ 0 & 0 & 0 & i \\ 0 & i\omega_p^2\epsilon_{\infty} & -i\omega_0^2 & -i\gamma \end{pmatrix} \begin{pmatrix} \mathbf{H} \\ \mathbf{E} \\ \mathbf{P} \\ \mathbf{J} \end{pmatrix} - \omega \begin{pmatrix} \mathbf{H} \\ \mathbf{E} \\ \mathbf{P} \\ \mathbf{J} \end{pmatrix} = \begin{pmatrix} 0 \\ \omega\epsilon_{\infty}^{-1}[\epsilon_{\text{res}} - \epsilon_{\text{bg}}]\mathbf{S}_{\text{ext}} \\ 0 \\ 0 \end{pmatrix}. \quad (\text{S.3.5})$$

Thirdly, with Eq. (S.3.2), we express $\omega\epsilon_{\infty}^{-1}[\epsilon_{\text{res}} - \epsilon_{\text{bg}}]\mathbf{S}_{\text{ext}}$ with

$$\omega\epsilon_{\infty}^{-1}[\epsilon_{\text{res}} - \epsilon_{\text{bg}}]\mathbf{S}_{\text{ext}} = \omega\epsilon_{\infty}^{-1}\Delta\epsilon_{\infty} + i\epsilon_{\infty}^{-1}\mathbf{J}_s, \quad (\text{S.3.6})$$

where

$$\mathbf{J}_s = -i\omega \frac{\Delta(\epsilon_{\infty}\omega_p^2)}{\omega^2 - \omega_0^2 + i\omega\gamma} \mathbf{S}_{\text{ext}}. \quad (\text{S.3.7})$$

Further, we introduce $\mathbf{P}_s = i\mathbf{J}_s/\omega$, and define that

$$\mathbf{P}' = \mathbf{P} + \mathbf{P}_s, \quad \mathbf{J}' = \mathbf{J} + \mathbf{J}_s, \quad (\text{S.3.8})$$

where we note that \mathbf{P} and \mathbf{J} are components of the augmented electromagnetic vector. Then, reexpressing Eq. (S.3.5) in terms of $\Psi' \equiv [\mathbf{H}, \mathbf{E}, \mathbf{P}', \mathbf{J}']$, we arrive at

$$\begin{pmatrix} 0 & -i\mu_0^{-1}\nabla\times & 0 & 0 \\ i\epsilon_{\infty}^{-1}\nabla\times & 0 & 0 & -i\epsilon_{\infty}^{-1} \\ 0 & 0 & 0 & i \\ 0 & i\omega_p^2\epsilon_{\infty} & -i\omega_0^2 & -i\gamma \end{pmatrix} \begin{pmatrix} \mathbf{H} \\ \mathbf{E} \\ \mathbf{P}' \\ \mathbf{J}' \end{pmatrix} - \omega \begin{pmatrix} \mathbf{H} \\ \mathbf{E} \\ \mathbf{P}' \\ \mathbf{J}' \end{pmatrix} = \begin{pmatrix} 0 \\ \omega\epsilon_{\infty}^{-1}\Delta\epsilon_{\infty}\mathbf{S}_{\text{ext}} \\ 0 \\ -i\Delta(\epsilon_{\infty}\omega_p^2)\mathbf{S}_{\text{ext}} \end{pmatrix}, \quad (\text{S.3.9})$$

being linear with respect to ω .

Lastly, we expand Ψ' in terms of the QNM vectors in the unperturbed system, $\widetilde{\Psi}_{u;n} \equiv [\widetilde{\mathbf{H}}_{u;n}, \widetilde{\mathbf{E}}_{u;n}, \widetilde{\mathbf{P}}_{u;n}, \widetilde{\mathbf{J}}_{u;n}]$:

$$\Psi' = \sum_n \beta_n \widetilde{\Psi}_u. \quad (\text{S.3.10})$$

By exploiting the orthogonal relation between the QNM eigenvectors (see Eq. (4) in Ref. [S1]), the expansion coefficients are given by

$$\beta_n(\omega) = - \iiint \widetilde{\mathbf{E}}_{u;n}(\mathbf{r}) \left[\frac{\omega \Delta \boldsymbol{\varepsilon}(\widetilde{\omega}_{u;n})}{\omega - \widetilde{\omega}_{u;n}} + \Delta \boldsymbol{\varepsilon}_\infty \right] \cdot \mathbf{S}_{\text{ext}}(\mathbf{r}) d^3 \mathbf{r}, \quad (\text{S.3.11})$$

where $\Delta \boldsymbol{\varepsilon}(\widetilde{\omega}_{u;n}) \equiv \boldsymbol{\varepsilon}_{\text{res}}(\widetilde{\omega}_{u;n}) - \boldsymbol{\varepsilon}_{\text{bg}}(\widetilde{\omega}_{u;n})$ and $\Delta \boldsymbol{\varepsilon}_\infty \equiv \lim_{\omega \rightarrow \infty} \boldsymbol{\varepsilon}_{\text{res}}(\omega) - \boldsymbol{\varepsilon}_{\text{res}}(\omega)$. Thus, the total electric field \mathbf{E} is given by

$$\mathbf{E}(\mathbf{r}; \omega) = - \sum_n \widetilde{\mathbf{E}}_{u;n}(\mathbf{r}) \iiint \widetilde{\mathbf{E}}_{u;n}(\mathbf{r}') \left[\frac{\omega \Delta \boldsymbol{\varepsilon}(\widetilde{\omega}_{u;n})}{\omega - \widetilde{\omega}_{u;n}} + \Delta \boldsymbol{\varepsilon}_\infty \right] \cdot \mathbf{S}_{\text{ext}}(\mathbf{r}') d^3 \mathbf{r}'. \quad (\text{S.3.12})$$

Comparing Eqs. (S.3.4) and (S.3.12) gives us the final result

$$\mathbf{G}_u(\mathbf{r}, \mathbf{r}'; \omega) [\boldsymbol{\varepsilon}_{\text{res}}(\omega) - \boldsymbol{\varepsilon}_{\text{bg}}(\omega)] = - \sum_n \widetilde{\mathbf{E}}_{u;n}(\mathbf{r}) \otimes \widetilde{\mathbf{E}}_{u;n}(\mathbf{r}') \left[\frac{\omega \Delta \boldsymbol{\varepsilon}(\widetilde{\omega}_{u;n})}{\omega - \widetilde{\omega}_{u;n}} + \Delta \boldsymbol{\varepsilon}_\infty \right], \quad (\text{S.3.13})$$

concluding this section.

IV. COMMENTS ON CONVENTIONAL PERTURBATION THEORIES

For the conventional perturbation theories, the fields in the perturbed domains are directly expanded with the QNM fields of the unperturbed system. This expansion itself is rigorous as long as the QNM basis is complete [S2]. However, the resulted perturbation theories are unable to deliver simple, correct perturbation series when fields are discontinuous across different media. Below, we shall elaborate this point thoroughly using both analytic arguments and numerical demonstrations.

Analytic arguments: Within the framework of the conventional perturbation theories, using our notations, Eq. (2a) in the main text keep intact, while Eq. (2b) changes to

$$\mathcal{H}_{\omega;nq} \simeq \left\langle \widetilde{\mathbf{E}}_{u;n}^{\text{P}*} \left| h \Delta \boldsymbol{\varepsilon}(\widetilde{\omega}_{u;n}) \right| \widetilde{\mathbf{E}}_{u;q}^{\text{P}} \right\rangle_{\partial \Omega_u}, \quad (\text{S.4.1})$$

which depends only on the QNM electric field at the perturbed side, i.e., $\widetilde{\mathbf{E}}_u^{\text{P}}$. As a result, for a non-degenerated mode, the QNM frequency shift, $\Delta \widetilde{\omega}_n \equiv \widetilde{\omega}_{p;n} - \widetilde{\omega}_{u;n}$, to the first order of the geometric deformation parameter h is expressed as

$$\Delta \widetilde{\omega}_n = - \left\langle \widetilde{\mathbf{E}}_{u;n}^{\text{P}*} \left| h \Delta \boldsymbol{\varepsilon}(\widetilde{\omega}_{u;n}) \right| \widetilde{\mathbf{E}}_{u;n}^{\text{P}} \right\rangle_{\partial \Omega_u} + \mathcal{O}(h^2). \quad (\text{S.4.2})$$

To make clear the deficiency of Eq. (S.4.2), we refer to a concrete case that a nanosphere resonator changes its radius from r_0 to r_1 , and, accordingly, there is $h = r_1 - r_0$. For $h > 0$, the perturbed side belongs to the background medium, so that we especially denote $\widetilde{\mathbf{E}}_{u;n}^{\text{P}}$ by $\widetilde{\mathbf{E}}_{u;n}^{\text{bg}}$ to indicate the position of the perturbed side; while for $h < 0$, the perturbed side belongs to the nanoresonator and we denote $\widetilde{\mathbf{E}}_{u;n}^{\text{P}}$ by $\widetilde{\mathbf{E}}_{u;n}^{\text{res}}$. Consequently, there is

$$\Delta \widetilde{\omega}_n = \begin{cases} -h \left\langle \widetilde{\mathbf{E}}_{u;n}^{\text{bg}*} \left| \Delta \boldsymbol{\varepsilon}(\widetilde{\omega}_{u;n}) \right| \widetilde{\mathbf{E}}_{u;n}^{\text{bg}} \right\rangle_{\partial \Omega_u} + \mathcal{O}(h^2) & h > 0 \\ -h \left\langle \widetilde{\mathbf{E}}_{u;n}^{\text{res}*} \left| \Delta \boldsymbol{\varepsilon}(\widetilde{\omega}_{u;n}) \right| \widetilde{\mathbf{E}}_{u;n}^{\text{res}} \right\rangle_{\partial \Omega_u} + \mathcal{O}(h^2) & h < 0 \end{cases}. \quad (\text{S.4.3})$$

We, thus, see that, when $\widetilde{\mathbf{E}}_{u;n}^{\text{bg}}$ and $\widetilde{\mathbf{E}}_{u;n}^{\text{res}}$ are different—a situation occurring for TM polarized modes, e.g., plasmonic modes, which have normal components of electric fields that are discontinuous across different

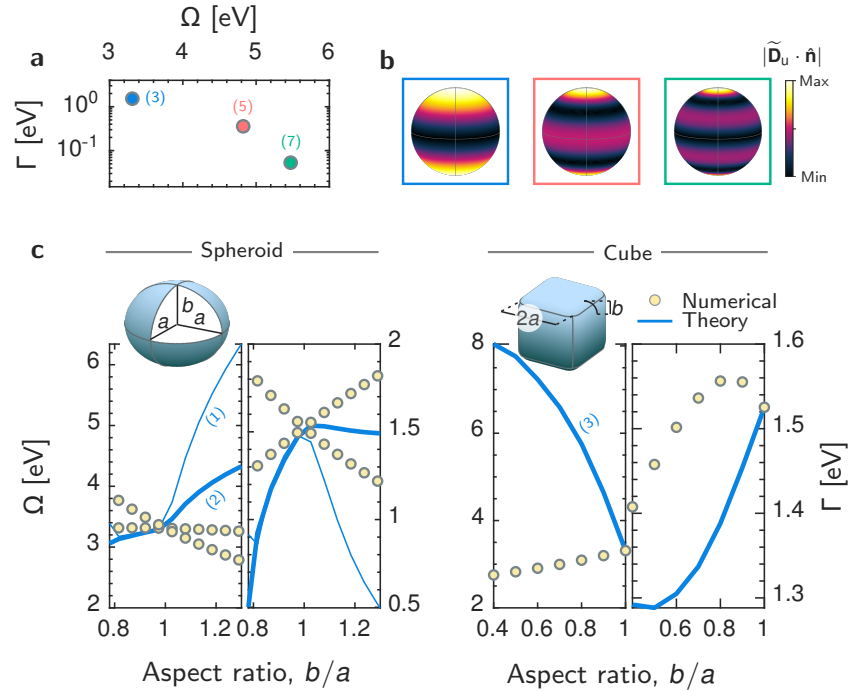


FIG. S1 **Deficiency of the conventional perturbation theories.** A metallic sphere with a radius of 50 [nm] in air background is deformed to spheroids and cubes. The sphere has a Drude permittivity $\epsilon_{\text{metal}} = 1 - \omega_p^2/(\omega^2 + i\omega\gamma)$ with $\hbar\omega_p = 9$ [eV] and $\gamma = 0.0023\omega_p$ close to Ag. **a.** Eigenfrequencies of dipole (blue), quadrupole (red), hexapole (green) plasmonic QNMs of the sphere, $\tilde{\omega}_u \equiv \Omega_u - i\Gamma_u/2$, including 15 QNMs with degeneracy factors labelled in parenthesis. **b.** Amplitudes of normal component of electric displacement fields at the metal-air boundary for dipole, quadrupole, hexapole (left to right) modes with azimuthal order $m = 0$. **c.** Eigenfrequencies of the metallic spheroids and cubes, $\tilde{\omega}_p \equiv \Omega_p - i\Gamma_p/2$, over a range of aspect ratios a/b with $a = 50$ [nm] (small deformations close to $a/b = 1$). The theoretical predictions (solid curves), with Eq. (2a) in the main text and Eq. (S.4.1) including 15 QNMs, disagree with the numerical results obtained with the QNMEig [S1] (circles).

media—, $\Delta\tilde{\omega}_n$ is not analytic at $h = 0$ since its first-order derivative with respect to h is discontinuous. However, for a continuous variation of the radius of the nanoresonator, $\Delta\tilde{\omega}_n$ should be generally analytic, which contradicts with the conclusion derived from the conventional perturbation theories and, thus, prove the deficiency of the latter.

Numerical demonstrations: We reconsider the numerical example in Fig. 1 in the main text, and compare the predictions from the conventional theories—i.e., using Eq. (2a) and Eq. (S.4.1), and retaining 15 QNMs—and from the fully-numerical simulations using the QNMEig [S1]. The results are plotted in Fig. S1, which evidence the degenerated numerical accuracy of the conventional theories as compared with our theory.

References

- * Electronic address: wyanzju@gmail.com
- † Electronic address: qiumin@westlake.edu.cn
- [S1] W. Yan, R. Faggiani, and P. Lalanne, Phys. Rev. B **97**, 205422 (2018).
- [S2] E. A. Muljarov and W. Langbein, Phys. Rev. B **94**, 235438 (2016).